

Computationally Tractable Robust Nonlinear Model Predictive Control using DC Programming

Martin Doff-Sotta*

Zaheen A-Rahman†

Mark Cannon‡

Abstract—We propose a computationally tractable, tube-based robust nonlinear model predictive control (MPC) framework using difference-of-convex (DC) functions and sequential convex programming. For systems with differentiable discrete time dynamics, we show how to construct systematic, data-driven DC model representations using polynomials and machine learning techniques. We develop a robust tube MPC scheme that convexifies the online optimization by linearizing the concave components of the model, and we provide guarantees of recursive feasibility and robust stability. We present three data-driven procedures for computing DC models and compare performance using a planar vertical take-off and landing (PVTOL) aircraft case study.

Keywords: Nonlinear Model Predictive Control; Non-convex Optimization; DC Programming; Data-driven Control.

1 Introduction

Robust model predictive control (MPC) is a receding-horizon optimal control strategy that provides guarantees of robust stability and constraint satisfaction for systems with uncertain dynamics [1, 2]. For nonlinear systems, dynamics are often difficult to identify accurately from data, while first-principles models typically contain unknown parameters, disturbances, and structural uncertainty. Uncertainty in the model used by the controller makes robustness guarantees essential for safe deployment. Achieving such guarantees, however, can lead to conservative designs and substantial computational effort. This paper develops a data-driven modelling and optimization framework for robust nonlinear MPC that improves the trade-off between computational cost and

conservatism.

Tube MPC addresses model uncertainty over the prediction horizon by constructing tubes that bound system trajectories. The approach is well established for linear systems [3, 2], but for nonlinear systems [4, 1, 5, 6, 7], robust uncertainty propagation remains a major obstacle to deployment. Existing nonlinear tube MPC methods often rely on restrictive structural assumptions (e.g. feedback linearizability) [5], computationally intensive offline designs (e.g. global contraction metrics) [6, 7], and general-purpose nonconvex solvers for the online MPC problem.

A common approach for nonlinear MPC for systems with differentiable dynamics is to linearize the model around previously predicted trajectories, yielding a sequence of convex approximations of the online optimization [8, 9]. With suitable bounds on linearization errors [10], such methods can provide recursive feasibility and robust stability guarantees using tools from robust linear MPC [11, 12]. Moreover, as sequential convex programming methods, they enjoy at least linear local rates of convergence [13]. However, the requirement for linearization error bounds can cause conservative approximations [10] or impose restrictive state and input constraints [11, 12].

When the system model is expressed as a difference of convex functions, the online MPC optimization can be formulated as a difference of convex (DC) programming problem [14]. This is a special case of sequential convex programming [13], but it avoids the difficulties of computing and incorporating linearization error bounds in the MPC optimization by exploiting the convex-concave procedure (CCP) [15, 16]. In particular, the CCP requires linearization of only the concave terms in constraints governing the propagation of tubes over the prediction horizon [14], leading to tight global bounds on model approximation errors and hence convergence to a local solution of the nonlinear MPC optimization [17]. Recursive feasibility and robust stability guarantees are available in the presence of model uncertainty and disturbances [18, 19, 17].

Although any system with continuous dynamics can in principle be approximated arbitrarily closely using dif-

*Department of Engineering Science, University of Oxford.
martin.doff-sotta@eng.ox.ac.uk

†St John’s College / Department of Engineering Science, University of Oxford. zaheen.a-rahman@sjc.ox.ac.uk

‡Department of Engineering Science, University of Oxford.
mark.cannon@eng.ox.ac.uk

ferences of smooth convex functions [20], first-principles models are not available in DC form except in special cases [14, 17]. Recent work has therefore proposed application-specific data-driven DC modelling approaches combined with physical models, using sum-of-squares convex (SOS-convex) polynomials [21, 22] and neural networks [23, 24, 25]. This paper provides a unifying theoretical framework and comparative numerical evaluation of these approaches for robust nonlinear MPC, including additional comparisons with a third method based on sums of radial basis functions.

The contributions of this paper are as follows: i) development of a computationally tractable robust MPC algorithm for nonlinear systems with continuous dynamics and additive disturbances; ii) presentation of data-driven techniques for deriving system models in DC form; iii) development of a method to guarantee recursive feasibility in case of additive disturbances; iv) numerical studies characterizing the performance of each algorithm.

The paper is organized as follows. Section 2 introduces data-driven DC modelling. Section 3 presents the tractable robust nonlinear MPC algorithm and tube parameterization. Section 4 extends this to the case of additive disturbances and introduces a backtracking line search to ensure recursive feasibility. Section 5 presents convergence and robust stability results. Section 6 evaluates performance in numerical studies, including a non-convex PVTOL example.

Notation: At the n th discrete time step, a variable $x \in \mathbb{R}^{n_x}$ is denoted $x[n]$, and a sequence predicted over horizon $n, \dots, n+N$ is denoted $\{x_k\}_{k=0}^N := \{x_0, \dots, x_N\}$, where x_k is the predicted value of $x[n+k]$. A symmetric matrix $P \in \mathbb{R}^{q \times q}$ is positive definite (or semidefinite) if $P \succ 0$ (or $P \succeq 0$), and the weighted Euclidean norm is $\|x\|_P := (x^\top Px)^{1/2}$. We denote $[f^\circ](x, u) = f(x^\circ, u^\circ) + A_k(x - x^\circ) + B_k(u - u^\circ)$ as the Jacobian linearization of f , with $A_k = (\partial f / \partial x)(x^\circ, u^\circ)$, $B_k = (\partial f / \partial u)(x^\circ, u^\circ)$. The l th element of a function $f : \mathbb{R}^p \rightarrow \mathbb{R}^q$ is denoted $[f]_l$ and f is called a DC function (or simply DC) if $f = g - h$, where $g, h : \mathbb{R}^p \rightarrow \mathbb{R}^q$ are such that $[g]_l, [h]_l$ are convex functions for $l = 1, \dots, q$. Optimization operations for vector-valued functions are intended componentwise, so if f is vector-valued, then $\max_x f(x)$ has l th element $\max_x [f(x)]_l$ for all l .

2 DC decomposition

2.1 Smooth dynamical systems

This paper considers nonlinear systems with dynamics

$$x[n+1] = f(x[n], u[n]), \quad (1)$$

where $x \in \mathbb{R}^{n_x}$, $u \in \mathbb{R}^{n_u}$ and $f : \mathbb{R}^{n_x} \times \mathbb{R}^{n_u} \rightarrow \mathbb{R}^{n_x}$ is continuous. Any twice-continuously-differentiable function f can be expressed in DC form [20] such that $f = g - h$, and any continuous function f can be approximated arbitrarily closely by a DC function on a compact convex set [26, 20]. We describe in the following sections three methods of obtaining an approximate DC representation. In what follows, we denote $x = [x_k^\top \ u_k^\top]^\top$.

2.2 SOS-convex polynomials

A DC decomposition can be obtained using polynomial approximation. We present here a method that applies to a multivariate scalar function to compute the DC decomposition $f = g - h$, where g, h are convex. This method applies to a large class of systems since: a) any continuous function can be approximated arbitrarily closely by a polynomial (Stone-Weierstrass theorem) and; b) any polynomial can be computed as a difference of convex polynomials of same degree [27].

- 1) *Fit polynomial to data.* We assume that the nonlinear model¹ f can be approximated arbitrarily closely by a polynomial of degree $2d$ in Gram form such that $f \approx y(x)^\top F y(x)$, where $F = F^\top$ is the Gram matrix and $y = [1, x_1, x_2, \dots, x_n, x_1 x_2, \dots, x_n^d]^\top$ is a vector of monomials of degree up to d (y has size $C_{d+|x|}^{|x|}$). Generating N_s samples $f_s = f(x_s), \forall s \in [1, \dots, N_s]$ of the nonlinear model, we solve the following least squares problem:

$$\min_F \sum_{s=0}^{N_s} \|f_s - y(x_s)^\top F y(x_s)\|_2^2, \quad \text{s.t. } F = F^\top.$$

- 2) *Compute the Hessians.* Let $g(x) \approx y(x)^\top G y(x)$ and $h(x) \approx y(x)^\top H y(x)$ be convex polynomials² such that their Hessians $d^2 g(x) / dx^2 = y(x)^\top G y(x)$ and $d^2 h(x) / dx^2 = y(x)^\top H y(x)$ are positive semidefinite (PSD). Finding G, H such that $F = G - H$ and $g(x), h(x)$ are convex reduces to solving a feasibility semidefinite program (SDP) with constraints $\mathcal{G} \succeq \sigma I$, $\mathcal{H} \succeq \sigma I$, $\sigma \geq 0$, where $\mathcal{G} := \sum_{i,j} (e_i e_j^\top) \otimes \mathcal{G}_{ij}$, $\mathcal{H} := \sum_{i,j} (e_i e_j^\top) \otimes \mathcal{H}_{ij}$ are block defined by $\forall i, j$

$$\begin{aligned} \mathcal{G}_{ij} &= D_{ji}^\top G + G D_{ij} + D_i^\top G D_j + D_j^\top G D_i, \\ \mathcal{H}_{ij} &= D_{ji}^\top (G - F) + (G - F) D_{ij} \\ &\quad + D_i^\top (G - F) D_j + D_j^\top (G - F) D_i, \end{aligned}$$

¹Note that it does not need to be a mathematical function but can be defined from data.

²In particular, they are SOS-convex polynomials following the terminology in [27]. SOS-convexity implies convexity and involves solving an SDP.

where I is the identity matrix of compatible dimensions, D_i is a matrix of coefficients such that $\partial y / \partial x_i = D_i y$, $D_{ij} = D_i D_j$ such that $\partial^2 y / \partial x_i \partial x_j = D_{ij} y$, and e_i is the basis vector of the appropriate dimensions.

Remark 1. In general, $f = [y^\top F_1 y, \dots, y^\top F_{n_x} y]^\top$, which requires computing n_x (offline) DC decompositions such that

$$f = \underbrace{\begin{bmatrix} y^\top G_1 y \\ \vdots \\ y^\top G_{n_x} y \end{bmatrix}}_g - \underbrace{\begin{bmatrix} y^\top H_1 y \\ \vdots \\ y^\top H_{n_x} y \end{bmatrix}}_h.$$

2.3 Input-convex neural networks

A neural network architecture with convex input-output map was introduced in [28]. The so called input-convex neural network (ICNN) is obtained by constraining the kernel weights of the network to be nonnegative at training stage and using convex activation functions. A fully connected L -layer feedforward ICNN with parameters $\theta = \{\Theta_{1:L-1}, \Phi_{0:L-1}, b_{0:L-1}\}$ and input-output map given by $z_L = f(x; \theta)$ can be defined by the following update equation $\forall l \in \{0, \dots, L-1\}$ (cf. Figure 1)

$$z_{l+1} = \sigma(\Theta_l z_l + \Phi_l x + b_l),$$

where z_l is the layer activation (with $z_0, \Theta_0 = 0$), Θ_l are positively constrained kernel weights ($\{\Theta_l\}_{ij} \geq 0, \forall i, j, \forall l \in \{1, \dots, L-1\}$), Φ_l are input weights, b_l are bias weights, and σ is a convex nondecreasing activation function (e.g. the ReLU function). Note that in order to allow sufficient representation power, the input is fed-back to each layer.

Alternatively, the network can be expressed as the composition of affine transformations $\mathcal{A}_{\theta_l, x}(z) = \Theta_l z + \Phi_l x + b_l, \forall l \in \{1, \dots, L-1\}$ and $\mathcal{A}_{\Phi_0}(x) = \Phi_0 x + b_0$ and convex nondecreasing activation function σ as follows

$$f(x; \theta) = (\sigma \circ \mathcal{A}_{\theta_{L-1}, x} \circ \dots \circ \sigma \circ \mathcal{A}_{\theta_1, x} \circ \sigma \circ \mathcal{A}_{\Phi_0})(x).$$

Each layer of an ICNN thus consists in the composition of a convex function with a nondecreasing convex function, which results in a convex map f between the input of the network and the output (see [29]). When the input and output are taken as $x = [x_k^\top \ u_k^\top]^\top$ and $z_L = x_{k+1}$, the network can be used to learn the dynamic function of a system.

Recently, a neural network model with DC structure was proposed in [30], and consists in two parallel ICNN whose outputs are subtracted. They also note that a

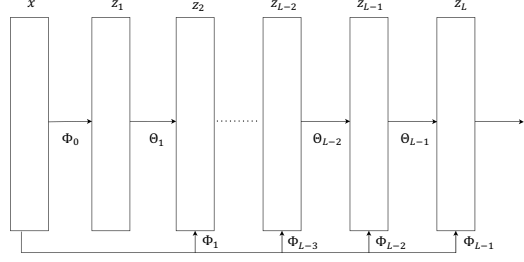


Figure 1: ICNN architecture $z_L = f(x; \theta)$ where the kernel weights Θ_l are nonnegative $\forall l \geq 1$ and activation functions are convex non-decreasing.

similar DC structure can be achieved with the same architecture in which the kernel weights Θ_{L-1} connecting the two last layers are unconstrained. Such a network (which we refer to as DCNN in the sequel) can be trained on data collected from "smooth" dynamical systems to learn the dynamics in DC form.

2.4 Radial basis functions

A radial basis function (RBF) is a function φ whose value depends only on the distance between its input x and some fixed point c (or centre), i.e. $\varphi(r) = \varphi(\|x - c\|)$ where $r = \|x - c\|$. A function $f \in \mathbb{R}^{n_x}$ can be efficiently approximated using weighted sums of RBF as follows

$$f = \sum_{j=0}^m \alpha_j \varphi(\|x - c_j\|_{\rho_j}),$$

where $\alpha_j \in \mathbb{R}^{n_x}$ are coefficients, $\rho_j \in \mathbb{S}_+^n$ are scaling matrices, and $c_j \in \mathbb{R}^n$ are centres.

If the RBF kernel is a convex function, then $f = g - h$ is DC where

$$g = \sum_{j=0}^m \max\{\alpha_j, 0\} \varphi(\|x - c_j\|_{\rho_j}),$$

$$h = - \sum_{j=0}^m \min\{\alpha_j, 0\} \varphi(\|x - c_j\|_{\rho_j}).$$

The following theorem gives sufficient conditions for a RBF to be convex.

Theorem 1 (Convex RBF). *A RBF $\varphi(r(x))$ where $r(x) = \|x - c\|$ is convex with respect to x if $\varphi'(r) \geq 0$ and $\varphi''(r) \geq 0$.*

Proof. By the second order convexity condition [29], the RBF φ is convex iff the Hessian is PSD, i.e. $\nabla^2 \varphi(x) \succeq 0, \forall x \in \mathbb{R}^n$.

By the chain rule, the gradient is given by

$$\nabla \varphi = \varphi'(r) \nabla r,$$

and the Hessian is

$$\nabla^2 \varphi = \varphi''(r) \nabla r (\nabla r)^\top + \varphi'(r) \nabla^2 r.$$

The Hessian is PSD iff, $\forall z \in \mathbb{R}^n$

$$\begin{aligned} z^\top \nabla^2 \varphi z \geq 0 &\Leftrightarrow \varphi''(r) z^\top \nabla r (\nabla r)^\top z + \varphi'(r) z^\top \nabla^2 r z \geq 0, \\ &\Leftrightarrow \varphi''(r) \|(\nabla r)^\top z\|_2^2 + \varphi'(r) z^\top \nabla^2 r z \geq 0, \end{aligned} \quad (2)$$

By convexity of the norm, $z^\top \nabla^2 r z \geq 0$, and since $\|(\nabla r)^\top z\|_2^2 \geq 0$, the Hessian is PSD if $\varphi''(r) \geq 0$ and $\varphi'(r) \geq 0$. \square

Example 1. An example of a convex RBF is the multi-quadratic function

$$\varphi(r) = \sqrt{1 + (\rho r)^2},$$

where ρ is a scaling parameter and $r = \|x - c\|$. A function f can thus be approximated as a weighted sum of such RBF as follows

$$f = \sum_{j=1}^m \alpha_j \sqrt{1 + \rho_j^2 (x - c_j)^\top (x - c_j)}.$$

Remark 2. There are several approaches to learning parameters c_j , ρ_j , α_j , $\forall j = 1, \dots, m$. Given c_j and ρ_j , the weights α_j can be obtained by solving a least squares problem. If all parameters are to be optimized together, algorithms similar to training of neural networks can be used [31].

3 Successive linearization tube-based MPC

In this section, we leverage the data-driven DC decomposition techniques in Section 2 to develop a robust TMPC algorithm for the nonlinear system in equation (1). The algorithm is based on successive linearization and exploits the convex structure in the dynamics to bound the effect of the linear approximation. The scheme results in a sequence of computationally tractable convex programs to be solved at each time step.

As per the classical TMPC paradigm, we consider a two degree of freedom control law of the form

$$u_k = v_k + K_k x_k, \quad (3)$$

where the feedback matrix K_k is obtained, e.g. by solving a dynamic programming recursion for the linearized

system (see Appendix A) and the feedforward control sequence v_k stabilizes the uncertain³ state trajectories within a “tube” whose cross sections are robustly invariant sets. The tube cross-sections \mathcal{X}_k are parameterized by polytopic sets (see Figure 2) with ν vertices $\mathcal{V}(\mathcal{X}_k) = \{x_k^{(1)}, \dots, x_k^{(\nu)}\}$, $\forall k \in [0, \dots, N]$. The vertices are function of variables $q_k \in \mathbb{R}^{n_q}$ such that

$$\mathcal{X}_k = \{x : \Gamma x \leq q_k\} = \text{Co}\{x_k^{(1)}, \dots, x_k^{(\nu)}\}$$

where Γ is a fixed matrix. In this paper, we consider two parameterizations:

- *Elementwise bounds.* Each element of the state vector is constrained by lower and upper bounds $[q_{1,k}, q_{2,k}]$ as follows: $[q_{1,k}]_l \leq [x_k]_l \leq [q_{2,k}]_l$, $\forall k, l$. Taking $\Gamma = [I \ -I]^\top$ where $I \in \mathbb{R}^{n_x \times n_x}$ is the identity matrix and partitioning $q_k = [q_{2,k}^\top \ -q_{1,k}^\top]^\top$ where $q_{1,k}, q_{2,k} \in \mathbb{R}^{n_x}$, the vertices are expressed as, $\forall k = 0, \dots, N$

$$\mathcal{V}(\mathcal{X}_k) = \{\hat{x} : [\hat{x}]_l = [q_{i,k}]_l, \forall i = 1, 2, \forall l = 1, \dots, n_x\}. \quad (4)$$

This parameterization results in $|\mathcal{V}(\mathcal{X}_k)| = 2^{n_x}$ vertices.

- *Simplex.* A simplex is a polytope with the smallest number of vertices in a given dimension. Let $\Gamma = [-I \ 1]^\top$ where $I \in \mathbb{R}^{n_x \times n_x}$ is the identity matrix, $1 \in \mathbb{R}^{n_x}$ is a vector of ones. Partitioning $q_k = [\alpha_k^\top \ \beta_k]^\top$ where variables $\alpha_k \in \mathbb{R}^{n_x}$ and $\beta_k \in \mathbb{R}$, and noting $\sigma_k = \beta_k + 1^\top \alpha_k$, the vertices can be expressed as

$$\mathcal{V}(\mathcal{X}_k) = \{-\alpha_k, -\alpha_k + e_1 \sigma_k, \dots, -\alpha_k + e_{n_x} \sigma_k\}, \quad (5)$$

where e_1, \dots, e_{n_x} are standard basis vectors of \mathbb{R}^{n_x} . This parameterization results in $|\mathcal{V}(\mathcal{X}_k)| = n_x + 1$ vertices.

Without loss of generality, the system in equation (1) can be expressed as

$$f_\Gamma(x_k, v_k + K_k x_k) \leq q_{k+1}, \quad f_\Gamma \in \mathcal{C}^0 \quad (6)$$

where $f_\Gamma = \Gamma f$.

In general, the function f_Γ is nonconvex, which would result in an intractable MPC optimization. However, using the DC decomposition techniques in Section 2, the \mathcal{C}^0 function can be expressed in DC form $f_\Gamma = g - h$ where g, h are convex. Inequality (6) can thus be relaxed

³The uncertainty arises from the linearization (model uncertainty) and from external disturbances (additive uncertainty) as in Section 4.

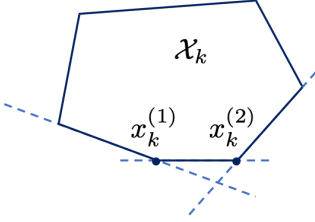


Figure 2: Polytopic tube cross section.

by linearizing the concave part of the DC decomposition around a predicted trajectory $(\mathbf{x}^\circ, \mathbf{u}^\circ)$ as follows

$$g(x_k, v_k + K_k x_k) - \lfloor h^\circ \rfloor(x_k, v_k + K_k x_k) \leq q_{k+1}. \quad (7)$$

By convexity, $\lfloor h^\circ \rfloor \leq h, \forall x_k$, (see Figure 3a for an illustration in \mathbb{R}) and we thus have the implication $(7) \Rightarrow (6)$. Crucially, inequality (7) is convex. We discuss computation of the Jacobian linearization of h for specific DC parameterizations in Appendix D.

In addition to the dynamical constraint (7), the state and input are constrained as follows

$$x_0 \in \mathcal{X}_0, \quad x_k \in \mathcal{X}, \quad x_N \in \hat{\mathcal{X}}, \quad v_k + K_k x_k \in \mathcal{U}, \quad (8)$$

for $k \in [0, \dots, N-1]$ where $\mathcal{X}_0, \mathcal{X}, \hat{\mathcal{X}}, \mathcal{U}$ are known convex compact sets. The terminal set $\hat{\mathcal{X}}$ can be defined simply as $\hat{\mathcal{X}} = \{x : \|x\|_{\hat{Q}} \leq \hat{\gamma}\}$ where $\hat{\gamma}$ is a terminal set bound. Appendix B provides a method based on semidefinite programming to compute the terminal parameters $\hat{\mathcal{X}}, \hat{Q}, \hat{\gamma}$ in order to guarantee the asymptotic stability result of Section 5.

The tube $\mathcal{X} = \{\mathcal{X}_k\}_{k=0}^N$ and feedforward control sequence $\mathbf{v} = \{v_k\}_{k=0}^{N-1}$ are variables in an optimal tracking control problem with constraints (7)-(8) and worst-case cost defined by

$$\begin{aligned} J(\mathbf{v}, \mathcal{X}) = & \sum_{k=0}^{N-1} \left[\max_{x_k \in \mathcal{X}_k} \|x_k - x_k^r\|_Q^2 \right. \\ & \left. + \max_{x_k \in \mathcal{X}_k} \|v_k + K_k x_k - u_k^r\|_R^2 \right] + \max_{x_N \in \mathcal{X}_N} \|x_N - x_N^r\|_{\hat{Q}}^2, \end{aligned} \quad (9)$$

where $R \succ 0, Q \succeq 0, \hat{Q} \succeq 0$ and x_k^r, u_k^r stand for reference state and input trajectories. This cost involves maximum operations over the sets \mathcal{X} . However, by convexity of the norm and since the sets \mathcal{X} are polytopes, these operations can be replaced by a discrete number of evaluations/comparisons of the norm functions at the vertices of the sets \mathcal{X} , which simplifies considerably the problem. This is because a convex function defined on a polytope achieves its maximum at one of the vertices (see

Appendix C and Figure 3b), so that maximization over a continuous space can be replaced by a discrete search. Following this idea, is thus tempting to parameterize the optimization problem in terms of the vertices of the tube.

Evaluation of the worst case cost can be achieved in practice by redefining it using slack variables θ, χ and introducing the vertices $\hat{x}_k \in \mathcal{V}(\mathcal{X}_k)$ as new optimization variables as follows

$$J = \theta_N^2 + \sum_{k=0}^{N-1} \theta_k^2 + \chi_k^2, \quad (10)$$

subject to $\forall k \in \{0, \dots, N-1\}, \forall \hat{x}_k \in \mathcal{V}(\mathcal{X}_k)$

$$\|\hat{x}_k - x^r\|_Q \leq \theta_k, \quad (11)$$

$$\|v_k + K_k \hat{x}_k - u^r\|_R \leq \chi_k, \quad (12)$$

and $\forall \hat{x}_N \in \mathcal{V}(\mathcal{X}_N)$

$$\|\hat{x}_N - x^r\|_{\hat{Q}} \leq \theta_N. \quad (13)$$

Note that the cost defined from equations (10)-(13) bounds the cost in equation (9).

The dynamic constraint in equation (7) can also be reformulated in terms of the vertices. By convexity of g , we have

$$\begin{aligned} q_{k+1} \geq & \max_{\hat{x}_k \in \mathcal{V}(\mathcal{X}_k)} g(\hat{x}_k, v_k + K_k \hat{x}_k) - \lfloor h^\circ \rfloor(\hat{x}_k, v_k + K_k \hat{x}_k), \\ \geq & \max_{x_k \in \mathcal{X}_k} g(x_k, v_k + K_k x_k) - \lfloor h^\circ \rfloor(x_k, v_k + K_k x_k), \\ \geq & g(x_k, v_k + K_k x_k) - \lfloor h^\circ \rfloor(x_k, v_k + K_k x_k), \end{aligned}$$

since a convex function defined on a polytope achieves its maximum at one of its vertices. This implies that $\forall \hat{x}_k \in \mathcal{V}(\mathcal{X}_k)$, inequality

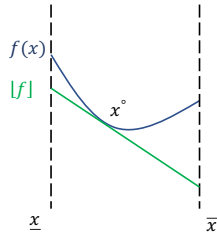
$$g(\hat{x}_k, v_k + K_k \hat{x}_k) - \lfloor h^\circ \rfloor(\hat{x}_k, v_k + K_k \hat{x}_k) \leq q_{k+1}, \quad (14)$$

enforces constraint (7).

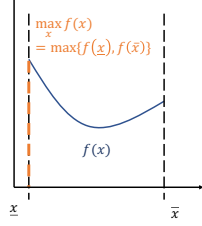
Finally, by convexity of the sets $\mathcal{X}_0, \mathcal{X}, \hat{\mathcal{X}}, \mathcal{U}$, the state and input constraints in (8) can be reformulated at the vertices as follows, $\forall \hat{x}_k \in \mathcal{V}(\mathcal{X}_k)$

$$\hat{x}_0 \in \mathcal{X}_0, \quad \hat{x}_k \in \mathcal{X}, \quad \hat{x}_N \in \hat{\mathcal{X}}, \quad v_k + K_k \hat{x}_k \in \mathcal{U}. \quad (15)$$

Gathering equation (10)-(15), the MPC optimization



(a) A convex function f (blue) defined on a compact set $[\underline{x}, \bar{x}]$ is bounded from below by its first order linear approximator $[f]$ (green).



(b) A convex function f (blue) defined on a compact set $[\underline{x}, \bar{x}]$ achieves its maximum (orange) at the boundary of the set.

Figure 3: Properties of a convex function

can be expressed as the following convex program

$$\begin{aligned} & \min_{\mathbf{v}, \mathcal{V}(\mathcal{X}), \boldsymbol{\theta}, \mathbf{x}, \mathbf{q}} \theta_N^2 + \sum_{k=0}^{N-1} \theta_k^2 + \chi_k^2 \\ & \text{subject to, } \forall k \in \{0, \dots, N-1\}, \forall \hat{x}_k \in \mathcal{V}(\mathcal{X}_k): \\ & \|\hat{x}_k - x^r\|_Q \leq \theta_k \\ & \|v_k + K_k \hat{x}_k - u^r\|_R \leq \chi_k \\ & g(\hat{x}_k, v_k + K_k \hat{x}_k) - \lfloor h^o \rfloor(\hat{x}_k, v_k + K_k \hat{x}_k) \leq q_{k+1} \\ & \hat{x}_k \in \mathcal{X} \\ & v_k + K_k \hat{x}_k \in \mathcal{U} \\ & \|\hat{x}_N - x^r\|_{\hat{Q}} \leq \theta_N \leq \sqrt{\gamma}, \forall \hat{x}_N \in \mathcal{V}(\mathcal{X}_N) \\ & \hat{x}_0 \in \mathcal{X}_0, \end{aligned} \quad (16)$$

where the variables q_k are related to $\mathcal{V}(\mathcal{X}_k)$ by equations (4) or (5) depending on the choice of polytopic parameterization.

Problem (16) is solved repeatedly and $(\mathbf{x}^o, \mathbf{u}^o)$ is updated according to

$$u_k^o \leftarrow v_k + K_k x_k^o, \quad (17a)$$

$$x_{k+1}^o \leftarrow f(x_k^o, u_k^o), \quad (17b)$$

for $k = 0, \dots, N-1$, and the process (16)-(17) is repeated until the maximum number of iterations is reached or

$\Delta J = J^{(j,n)} - J^{(j-1,n)}$ has converged to a sufficiently small value, where $J^{(j,n)}$ denotes the objective value at iteration j and time n . The control law is then implemented as

$$u[n] = u_0^o, \quad (18)$$

and at the subsequent discrete time instant we set $x_0^o \leftarrow x[n+1]$, and redefine $(\mathbf{x}^o, \mathbf{u}^o)$ for $k = 0, \dots, N-1$, by

$$u_k^o \leftarrow u_{k+1}^o, \quad (19a)$$

$$x_{k+1}^o \leftarrow f(x_k^o, u_k^o), \quad (19b)$$

$$u_{N-1}^o \leftarrow \hat{K}(x_{N-1}^o - x^r) + u^r, \quad (19c)$$

$$x_N^o \leftarrow f(x_{N-1}^o, u_{N-1}^o). \quad (19d)$$

where \hat{K} is a terminal gain matrix that can be computed e.g. as explained in Appendix B. These definitions ensure recursive feasibility of the scheme. In addition, the optimal value of $J(\mathbf{v}, \mathcal{X})$ is non-increasing at successive iterations, implying that the iteration converges asymptotically: $\mathbf{v} \rightarrow \mathbf{u}^o - K\mathbf{x}^o$ and $\mathcal{X} \rightarrow \mathbf{x}^o$, and also non-increasing at successive times $n = 0, 1, \dots$, implying that $(x, u) = (x^r, u^r)$ is an asymptotically stable equilibrium (see Section 5 for details).

The TMPC strategy for continuous systems is summarized in Algorithm 1.

Remark 3. When choosing a parameterization of the tube by means of elementwise bounds, the number of inequalities defining the tube in (14) grows exponentially with the number of states n_x : $|\mathcal{V}(\mathcal{S})| = 2^{n_x}$ vertices. That growth is further exacerbated if higher dimensional polytopes are used. In practice, most systems have a reasonable number of states. Moreover, prior knowledge of the state coefficients appearing linearly in these inequalities can potentially be exploited to reduce the number of inequalities. Finally, if computational burden is an issue, simplex sets can be used that scale linearly with the number of states: only $n_x + 1$ inequalities are needed.

Remark 4. The present TMPC strategy requires knowledge of a feasible predicted trajectory at time $n = 0$, namely a sequence $(\mathbf{x}^o, \mathbf{u}^o)$ satisfying $(x_k^o, u_k^o) \in \mathcal{X} \times \mathcal{U}$, $k = 0, \dots, N-1$ and $\|x_N^o - x^r\|_{\hat{Q}}^2 \leq \hat{\gamma}$. An iterative approach to determining a feasible trajectory can be constructed by relaxing some of the constraints of (16) and performing successive optimizations to minimize constraint violations. For example, given a trajectory $(\mathbf{x}^o, \mathbf{u}^o)$ of (1) that satisfies $(x_k^o, u_k^o) \in \mathcal{X} \times \mathcal{U}$, $k = 0, \dots, N-1$, but not the terminal constraint $\|x_N^o - x^r\|_{\hat{Q}}^2 \leq \hat{\gamma}$, a suitable iteration can be constructed by replacing $\hat{\gamma}$ in (16) with an optimization variable γ and replacing the objective of (16) with γ . Repeatedly solving this convex program and updating $(\mathbf{x}^o, \mathbf{u}^o)$ using (17a-b) will generate a convergent sequence of predicted

trajectories with non-increasing values of $\|x_N^o - x^r\|_{\hat{Q}}^2$, which can be terminated when $\gamma \leq \hat{\gamma}$ is achieved.

Algorithm 1: Successive linearization tube-based MPC.

```

1 Initialization
2   | Compute  $\hat{K}$ ,  $\hat{Q}$ ,  $\hat{\gamma}$  as in Appendix B
3 end
4 Online at times  $n = 0, 1, \dots$ 
5   | Set  $x_0^o \leftarrow x[n]$ 
6   | if  $n = 0$  then
7     |   | Find  $(\mathbf{x}^o, \mathbf{u}^o)$  such that  $x_{k+1}^o = f(x_k^o, u_k^o)$ ,
8     |   |  $(x_k^o, u_k^o) \in \mathcal{X} \times \mathcal{U}$  for  $k = 0, \dots, N-1$ , and
9     |   |  $\|x_N^o - x^r\|_{\hat{Q}}^2 \leq \hat{\gamma}$ 
10    | else
11      |   | Compute  $(\mathbf{x}^o, \mathbf{u}^o)$  using (19a-d)
12    | end
13    | Set  $\Delta J \leftarrow \infty$ ,  $j \leftarrow 0$ 
14    | while  $\Delta J > \text{tolerance}$  &  $j < \text{maxIters}$  do
15      |   | Linearize  $h$  around  $(\mathbf{x}^o, \mathbf{u}^o)$  to obtain  $[h^o]$ 
16      |   | Compute  $\{K_k\}_{k=0}^{N-1}$  as in Appendix A
17      |   | Solve (16) to find the optimal  $\mathbf{v}$  and  $\mathcal{X}$ 
18      |   | Update  $(\mathbf{x}^o, \mathbf{u}^o)$  using (17a-b)
19      |   | Update the objective:  $J^{(j,n)} \leftarrow J(\mathbf{v}, \mathcal{X})$ 
20      |   | Update the iteration counter:  $j \leftarrow j + 1$ 
21    | end
22    | Update the control input:  $u[n] \leftarrow u_0^o$ 
23 end

```

4 Additive disturbances

The algorithm presented in this paper can also be applied (with minor adjustments) to systems subject to additive uncertainty

$$x[n+1] = g(x[n], u[n]) - h(x[n], u[n]) + w[n], \quad w[n] \in \mathcal{W}, \quad (20)$$

where g, h are convex, w is a bounded disturbance and $\mathcal{W} \subset \mathbb{R}^{n_x}$ is a known compact set.

4.1 Terminal weighting matrix computation

The method in Appendix B has to be adapted to account for the impact of the disturbance on the terminal parameters. Equation (26) is relaxed $\forall x \in \hat{\mathcal{X}}$ by

$$\begin{aligned} \|x - x^r\|_{\hat{Q}}^2 &\geq \|f(x, \hat{K}(x - x^r) + u^r) - x^r\|_{\hat{Q}}^2 \\ &\quad + \|x - x^r\|_Q^2 + \|\hat{K}(x - x^r)\|_R^2 - \beta, \end{aligned} \quad (21)$$

where $\hat{Q} \succ 0$ is computed for some $\beta \geq 0$. The reader is referred to [19] for a method to compute \hat{Q} and the other terminal parameters in this scenario.

4.2 Predicted trajectory

Since the system is perturbed by additive disturbances whose future magnitude is uncertain, the trajectories of system (20) under a known control law are uncertain. Therefore, the tube bounding predicted states cannot converge to a single trajectory as in the undisturbed case. To guarantee recursive feasibility at each iteration of the scheme, a feasible predicted trajectory should be computed as part of a feasible tube as suggested in [18] to enforce constraint satisfaction under all realizations of the additive uncertainty. However this modification would complexify the algorithm significantly. As an alternative, we propose a heuristic based on a backtracking line search, under the assumption that predicted trajectories closer to the last feasible one are more likely to remain feasible. If the optimization problem at time $n > 0$ becomes infeasible due to external disturbances affecting the current state of the system, the problem can be reattempted by redefining the optimal control sequence obtained in equation (19a) by

$$\begin{pmatrix} x_0^o \\ \mathbf{v}^o \end{pmatrix} \leftarrow \begin{pmatrix} \bar{x}_0^o \\ \bar{\mathbf{v}}^o \end{pmatrix} + \rho \begin{pmatrix} x_0^o - \bar{x}_0^o \\ \mathbf{v}^o - \bar{\mathbf{v}}^o \end{pmatrix}, \quad (22)$$

before updating the initial guess with equations (19b-d), where $\rho \in]0, 1[$, \bar{x}_0^o denotes the state at the current timestep in the most recently obtained feasible state sequence, and $\bar{\mathbf{v}}^o$ stands for the last feasible feedforward control sequence starting from the current timestep. If the first iteration is infeasible, \mathbf{v}^o is set to the tail of the feasible feedforward control sequence at previous time $n-1$ (i.e. $(v_1^o, \dots, v_{N-1}^o, u^r)$); if there exists a feasible iteration at the current timestep, \mathbf{v}^o is set to the feedforward control sequence from the most recent such iteration. This process is repeated until the optimization problem can be solved. In the limit of infinite iterations, the new guess state and control sequences tend to either the necessarily feasible tails at time $n-1$, or the feasible sequences from the most recent feasible iteration at the current timestep. It is worth noting that ρ need not be a constant, indeed the only condition is that $\rho \in]0, 1[$.

4.3 Optimization with additive disturbance

Optimization problem (16) can be modified to account for the external disturbance as follows

$$\begin{aligned}
& \min_{\mathbf{v}, \mathcal{V}(\mathbf{X}), \boldsymbol{\theta}, \mathbf{x}, \mathbf{q}} \theta_N^2 + \sum_{k=0}^{N-1} \theta_k^2 + \chi_k^2 \\
& \text{subject to, } \forall k \in \{0, \dots, N-1\}, \forall \hat{x}_k \in \mathcal{V}(\mathcal{X}_k): \\
& \|\hat{x}_k - x^r\|_Q \leq \theta_k \\
& \|v_k + K_k \hat{x}_k - u^r\|_R \leq \chi_k \\
& g(\hat{x}_k, v_k + K_k \hat{x}_k) - \lfloor h^r \rfloor (\hat{x}_k, v_k + K_k \hat{x}_k) + \bar{w}_k \leq q_{k+1} \\
& \hat{x}_k \in \mathcal{X} \\
& v_k + K_k \hat{x}_k \in \mathcal{U} \\
& \|\hat{x}_N - x^r\|_{\hat{Q}} \leq \theta_N \leq \sqrt{\hat{\gamma}}, \forall \hat{x}_N \in \mathcal{V}(\mathcal{X}_N) \\
& \hat{x}_0 \in \mathcal{X}_0,
\end{aligned} \tag{23}$$

where $\bar{w}_k = \max_{w_k \in \mathcal{W}} \Gamma w_k$ depend on the tube parameterization and can trivially be computed via a discrete search over all vertices of \mathcal{W} if \mathcal{W} is a polytopic convex set.

4.4 Algorithm with additive disturbances

In the presence of external disturbance, the successive linearization tube-based MPC procedure is given in Algorithm 2. This algorithm is as described in Section 4, with one important note. In the case where `maxIters` = 1, the step where $x_0^o \leftarrow x[n]$ is skipped to ensure recursive feasibility of the algorithm, as the new trajectory generated from keeping the tail of the previous timestep's trajectory is guaranteed to be feasible. This is identical to skipping the first $x_0^o \leftarrow x[n]$ step and immediately entering a backtracking algorithm with $\rho \rightarrow 1$.

4.5 Accounting for modelling error in f

There always exists some modelling error when finding an arbitrarily close approximation to $f = g - h$. To account for this uncertainty, the disturbance set is augmented via the Minkowski sum $\mathcal{W} = \overline{\mathcal{W}} + \mathcal{E}$, where $\overline{\mathcal{W}}$ is a polytopic convex set of additive disturbances and \mathcal{E} is a polytopic convex set of maximum absolute modelling errors. The resulting set \mathcal{W} remains polytopic and convex since the Minkowski sum preserves these properties [32].

5 Theoretical results

This section establishes some important properties of the proposed algorithms. The results of this Section apply as long as the nonlinear dynamics can be approximated arbitrarily closely by the DC approximation model. If the

Algorithm 2: Successive linearization tube-based MPC (with external disturbances)

```

1 Initialization
2   | Compute  $\hat{K}$ ,  $\hat{Q}$ ,  $\hat{\gamma}$  as in [19]
3 end
4 Online at times  $n = 0, 1, \dots$ 
5   if  $n = 0$  then
6     | Set  $x_0^o \leftarrow x[n]$ 
7     | Find  $(\mathbf{x}^o, \mathbf{u}^o)$  such that  $x_{k+1}^o = f(x_k^o, u_k^o)$ ,
      |  $(x_k^o, u_k^o) \in \mathcal{X} \times \mathcal{U}$  for  $k = 0, \dots, N-1$ , and
      |  $\|x_N^o - x^r\|_{\hat{Q}}^2 \leq \hat{\gamma}$ 
8   else
9     | if maxIters > 1 then
10       | | Set  $x_0^o \leftarrow x[n]$ 
11     | end
12     | Compute  $(\mathbf{x}^o, \mathbf{u}^o)$  using (19a-d)
13   end
14   Set  $\Delta J \leftarrow \infty$ ,  $j \leftarrow 0$ 
15   while  $\Delta J > \text{tolerance}$  &  $j < \text{maxIters}$  do
16     | Linearize  $h$  around  $(\mathbf{x}^o, \mathbf{u}^o)$  to obtain  $\lfloor h^r \rfloor$ 
17     | Compute  $\{K_k\}_{k=0}^{N-1}$  as in Appendix A
18     | Solve (23) to find the optimal  $\mathbf{v}$  and  $\mathbf{X}$ 
19     | Set  $\rho$ 
20     | while  $\mathbf{v} = \{\emptyset\}$  &  $n > 0$  do
21       | | Recompute  $(\mathbf{x}^o, \mathbf{v}^o)$  using (22) and
          | | (17b-d)
22       | | Recompute  $\mathbf{u}^o$  using (17a)
23       | | Reattempt solving (23)
24     | end
25     | Update  $(\mathbf{x}^o, \mathbf{u}^o)$  using (17a-b)
26     | Update the objective:  $J^{(j,n)} \leftarrow J(\mathbf{v}, \mathbf{X})$ 
27     | Update the iteration counter:  $j \leftarrow j + 1$ 
28   | end
29   | Update the control input:  $u[n] \leftarrow u_0^o$ 
30 end

```

approximation errors are significant, they can be estimated and treated as bounded additive disturbances.

We first consider the case of no external disturbance, then provide modifications of the theorems in case of additive disturbances.

5.1 No external disturbances

We first show that $(\mathbf{x}^o, \mathbf{u}^o)$ is a feasible predicted trajectory at every iteration of Algorithm 1 and at all times $n \geq 0$. This ensures firstly that problem (16) is recursively feasible, and second that the while loop in line 12 of Algorithm 1 can be terminated after any number of iterations without compromising the stability of the MPC law, i.e. the approach allows *early termination* of

the MPC optimization.

Proposition 2 (Feasibility). *Assuming initial feasibility at time $n = 0$ and iteration $j = 0$, problem (16) in Algorithm 1 is feasible at all times $n > 0$ and all iterations $j > 0$.*

Proof. If $(\mathbf{x}^\circ, \mathbf{u}^\circ)$ is a feasible trajectory, namely a trajectory of (1) satisfying $(x_k^\circ, u_k^\circ) \in \mathcal{X} \times \mathcal{U}$, $k = 0, \dots, N-1$ and $\|x_N^\circ - x^r\|_Q^2 \leq \hat{\gamma}$, then problem (16) is feasible since $(\mathbf{v}, \mathbf{X}) = (\mathbf{u}^\circ - \mathbf{K}\mathbf{x}^\circ, \{\mathbf{x}^\circ\})$ trivially satisfies all constraints of (16). Furthermore, line 7 of Algorithm 1 requires that $(\mathbf{x}^\circ, \mathbf{u}^\circ)$ is a feasible trajectory at $n = 0$, and thus ensures that (16) in line 15 is feasible for $n = 0$, $j = 0$. Therefore $(\mathbf{x}^\circ, \mathbf{u}^\circ)$ computed in lines 9 and 16 of Algorithm 1 are necessarily feasible trajectories for all $n \geq 0$ and $j \geq 0$. \square

We next show that, at a given time n , the optimal values of the objective function for problem (16) computed at successive iterations of Algorithm 1 are non-increasing.

Lemma 3. *The cost $J^{j,n}$ in line 17 of Algorithm 1 satisfies $J^{j+1,n} \leq J^{j,n}$ for all $j \geq 0$.*

Proof. This is a consequence of the recursive feasibility of problem (16) in line 15 of Algorithm 1 as demonstrated by Proposition 2. Specifically, $J(\mathbf{v}, \mathbf{X})$ is the maximum of a quadratic cost evaluated over the predicted tube, so the feasible suboptimal solution $(\mathbf{v}, \mathbf{X}) = (\mathbf{u}^\circ - \mathbf{K}\mathbf{x}^\circ, \{\mathbf{x}^\circ\})$ at iteration $j+1$ must give a cost no greater than $J^{j,n}$. Therefore the optimal value at $j+1$ satisfies $J^{j+1,n} \leq J^{j,n}$. \square

Lemma 3 implies that $J^{j,n}$ converges to a limit as $j \rightarrow \infty$, and this is the basis of the following result, which implies convergence of the linearization error to zero.

Proposition 4 (Convergence). *The solution of (16) in Algorithm 1 at successive iterations at a given time n satisfies $(\mathbf{v}, \mathbf{X}) \rightarrow (\mathbf{u}^\circ - \mathbf{K}\mathbf{x}^\circ, \{\mathbf{x}^\circ\})$ as $j \rightarrow \infty$.*

Proof. From $J^{j,n} \geq 0$ and $J^{j+1,n} \leq J^{j,n}$ for all j , it follows that $J^{j,n}$ converges to a limit as $j \rightarrow \infty$. Since $Q \succ 0$ and $R \succ 0$, this implies that $\mathbf{v} \rightarrow \mathbf{u}^\circ - \mathbf{K}\mathbf{x}^\circ$ and \mathbf{x}° in the update (17a-d) in line 16 must also converge. Furthermore, since (\mathbf{v}, \mathbf{X}) minimizes the worst-case cost evaluated for the predicted tube, the optimal solutions of (16) must satisfy $\mathbf{X} \rightarrow \{\mathbf{x}^\circ\}$ as $j \rightarrow \infty$. \square

We finally show that under Algorithm 1, the closed loop is asymptotically stable.

Theorem 5 (Asymptotic stability). *For a system in DC form controlled by Algorithm 1, $x = x^r$ is an asymptotically stable equilibrium with region of attraction equal to*

the set of initial states $x[0]$ for which a feasible initial trajectory $(\mathbf{x}^\circ, \mathbf{u}^\circ)$ exists.

Proof. Let $(\mathbf{x}^\circ, \mathbf{u}^\circ)$ be the trajectory computed in line 9 of Algorithm 1 at $n+1$, for any initial state such that line 7 is feasible. Then, setting $(\mathbf{v}, \mathbf{X}) \rightarrow (\mathbf{u}^\circ - \mathbf{K}\mathbf{x}^\circ, \{\mathbf{x}^\circ\})$, and using $\mathcal{X}_0 = \{x_0^\circ\}$ and the descent property (26) of \hat{Q} , we obtain

$$J(\mathbf{v}, \mathbf{X}) \leq J^{j_n,n} - \|x[n] - x^r\|_Q^2 - \|u[n] - u^r\|_R^2,$$

where j_n is the final iteration count of Algorithm 1 at time n . The optimal solutions of (16) at time $n+1$ therefore give

$$J^{j_{n+1},n+1} \leq J^{0,n+1} \leq J^{j_n,n} - \|x[n] - x^r\|_Q^2 - \|u[n] - u^r\|_R^2.$$

Furthermore $J^{j,n}$ is a positive definite function of $x[n] - x^r$ since $Q \succ 0$, $R \succ 0$, and Lyapunov's direct method therefore implies that $x = x^r$ is asymptotically stable. \square

5.2 Additive disturbances

In the presence of additive disturbances, the following theorems apply.

Proposition 6 (Feasibility with disturbance). *Assuming initial feasibility at time $n = 0$ and iteration $j = 0$, problem (23) in Algorithm 2 is feasible at all times $n > 0$ and all iterations $j > 0$.*

Proof. See [19] for a proof. \square

Theorem 7 (Stability with disturbance). *The control law of Algorithm 2 ensures that the system (20) satisfies the state and input constraints and the following quadratic stability condition on the average stage cost:*

$$\lim_{t \rightarrow \infty} \frac{1}{t} \sum_{n=0}^{t-1} \|x[n] - x^r\|_Q^2 + \|u[n] - u^r\|_R^2 \leq \beta,$$

where β satisfies equation (21).

Proof. From (21) the cost satisfies

$$J^{j_{n+1},n+1} \leq J^{j_n,n} - \|x[n] - x^r\|_Q^2 - \|u[n] - u^r\|_R^2 + \beta,$$

where $J^{j_n,n}$ is the cost at final iteration for time n . This yields after summation, and by the telescopic sum

$$\begin{aligned} & \frac{1}{t} (J^{j_{t-1},t-1} - J^{j_0,0}) \\ & + \frac{1}{t} \sum_{n=0}^{t-1} (\|x[n] - x^r\|_Q^2 + \|u[n] - u^r\|_R^2) \leq \beta. \end{aligned}$$

Finally taking the limit as $t \rightarrow \infty$ yields

$$\lim_{t \rightarrow \infty} \frac{1}{t} \sum_{n=0}^{t-1} (\|x[n] - x^r\|_Q^2 + \|u[n] - u^r\|_R^2) \leq \beta,$$

which guarantees a finite bound on the averaged stage cost. \square

It follows from Theorem 7 that the objective of the MPC optimization is finite because the cost function has a finite number of stages and each stage cost is finite.

6 Numerical results

The simulation code for the tube-based MPC with DCNN decomposition is available at <https://github.com/martindoff/DC-NN-MPC>.

6.1 Case study

We consider the model of a planar vertical take-off and landing (PVTOL) aircraft as follows [11]

$$\ddot{y} = (u_1 + g) \sin \alpha, \quad \ddot{z} = (u_1 + g) \cos \alpha - g, \quad \ddot{\alpha} = u_2,$$

where y, z, α are the horizontal, vertical and angular displacement, $g = 9.81 \text{ m/s}^2$ is the acceleration due to gravity, u_1, u_2 are proportional to the net thrust and torque acting on the aircraft. The system is constrained as follows: $|u_1| \leq 10, |u_2| \leq 10, |\alpha| \leq 3, |\dot{\alpha}| \leq 1, |\dot{y}| \leq 30, |\dot{z}| \leq 10$. The dynamics are discretized with time step δ and the state is defined as $x = [y \ z \ \alpha \ \dot{y} \ \dot{z} \ \dot{\alpha}]^\top$ and input as $u = [u_1 \ u_2]^\top$. The penalty parameters are taken as $Q = \text{diag}(10, 1, 1, 1)$, $R = \text{diag}(1e-4, 1e-3)$, the bounds on terminal state and input (cf. Appendix B) are $\delta^x = [3e-2 \ 1 \ 1 \ 1e-1]^\top$, $\delta^u = [1 \ 1]^\top$, the initial conditions are $x_0 = [0.1 \ 0 \ 0 \ 0]^\top$, and the system is stabilized around the origin.

To exploit the linear structure in the dynamics, in what follows we only decompose the nonconvex part of the dynamics

$$f = \begin{bmatrix} \ddot{y} \\ \ddot{z} \end{bmatrix} = \begin{bmatrix} (u_1 + g) \sin \alpha \\ (u_1 + g) \cos \alpha - g \end{bmatrix}, \quad (24)$$

and treat the rest of the dynamics as linear constraints in optimization problem (16).

6.2 DC decomposition

We first analyse the performance of the different DC decomposition methods in Section 2 to approximate the

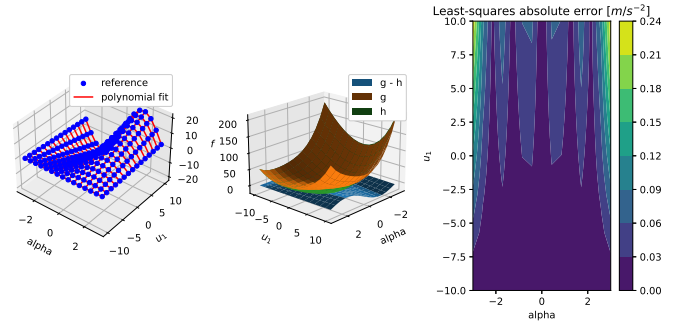


Figure 4: Approximation of the PVTOL horizontal dynamics as a difference of SOS-convex polynomials.

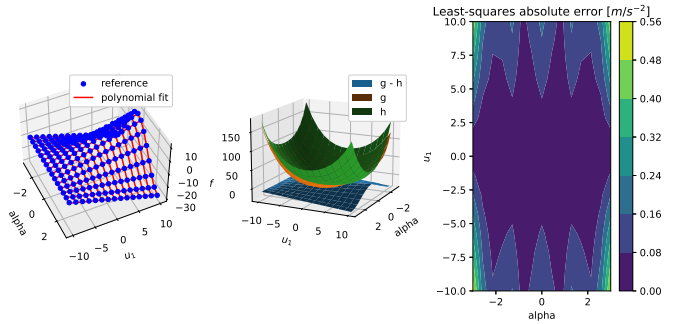


Figure 5: Approximation of the PVTOL vertical dynamics as a difference of SOS-convex polynomials.

nonconvex part of the PVTOL dynamics in equation (24) as $f = g - h$ where g, h are convex (we then exploit *a priori* knowledge of the uncertainty set parameterization matrix Γ in (6) to obtain a set of convex inequalities (14)).

6.2.1 SOS-convex polynomials

We fit two polynomials of degree $2d = 6$ on 100,000 samples generated from the PVTOL horizontal and vertical dynamics \ddot{y} and \ddot{z} . The results of the DC decompositions are shown in Figures 4 and 5. 100 test samples were generated and the mean absolute error (MAE) between the polynomial approximation and the mathematical model was 0.027 for \ddot{y} and 0.06 for \ddot{z} .

6.2.2 Input-convex neural networks

The DCNN architecture was leveraged in the present case study of the PVTOL aircraft model using the open-source neural-network library Keras [33]. The network has 1 hidden layer, 64 units and ReLU activation and was trained on 100,000 input-output samples generated randomly from the PVTOL model with the RMSprop

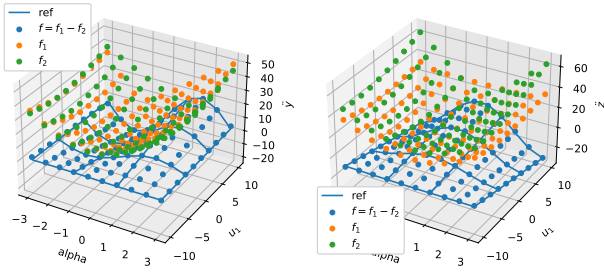


Figure 6: Approximation of the PVTOL model as a difference of convex functions by a DCNN.

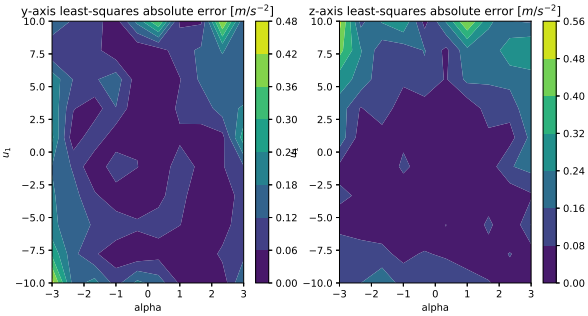


Figure 7: PVTOL aircraft model approximation error (MAE) with DCNN.

optimizer, MSE loss, batch size of 32, 200 epochs. An accuracy of 0.08 was obtained on 100 test samples with a MAE metrics (see Figure 7). The results of the approximation of the nonconvex dynamic function of the PVTOL aircraft by a DCNN are presented in Figure 6. The nonconvex dynamics (blue) are approximated by the DCNN as a difference of two convex functions (green and orange dots).

6.2.3 Radial basis functions

A sum of 49 radial basis functions with multiquadric kernel is fitted on 100,000 samples from the PVTOL model. This can be achieved by training a single layer neural network with multiquadric activation (as previously using RMSprop, MSE loss, batch of 64 and 100 epochs). The resulting accuracy (MAE) is 1.63 on 100 samples.

6.3 Effect of DC decomposition on closed-loop solution

We now compare the choice of DC decomposition on the closed-loop solution. We simulate the PVTOL aircraft

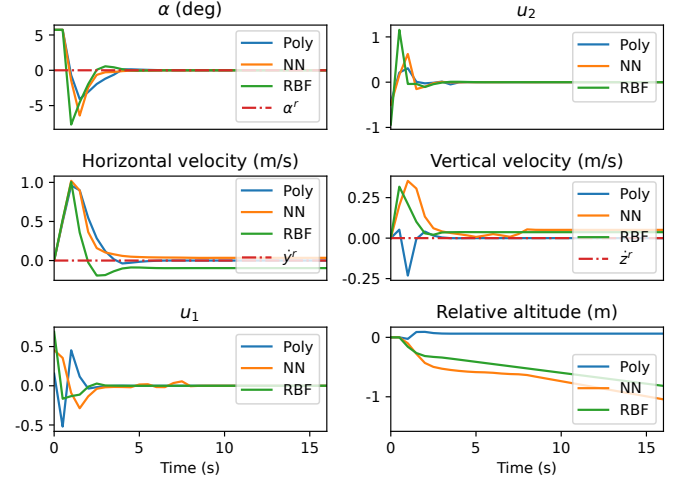


Figure 8: Comparison of closed-loop solution for each DC decomposition.

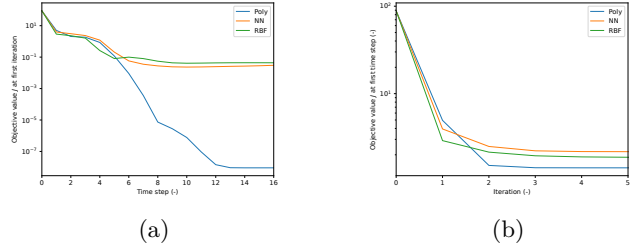


Figure 9: Comparison of objective evolution for each DC decomposition.

problem with a horizon $N = 50$, time step $\delta = 0.5 \text{ s}$, elementwise bounds parameterization, maximum number of iterations 1, and compare for each configuration the time response in Figure 8 and objective evolution (a measure of how close the system is from the reference) in Figure 9a. The polynomial DC decomposition results in the fastest convergence without much steady state error.

Setting the maximum number of iterations to `maxIters = 5`, we compare the evolution of the objective at the first time step in Figure 9b. Again, the polynomial decomposition yields the fastest convergence.

Simulating the problem for multiple time horizon values N , the average time to completion per iteration as a function of problem dimension is compared for each decomposition in Figure 10. The polynomial decomposition is usually the fastest method, followed closely by the neural-network decomposition. The RBF decomposition is significantly slower. These results must be nuanced by the facts that: i) CVXPY was used as the interface for the MOSEK solver, but specialized solvers might yield better performance (e.g. with ADMM, an improvement

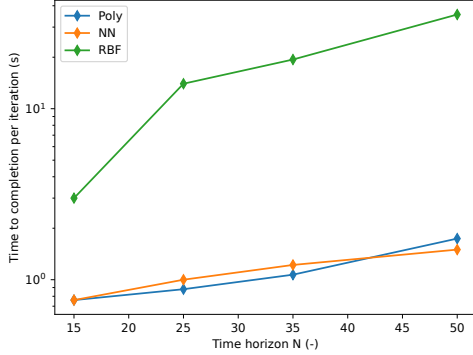


Figure 10: Comparison of time to completion as a function of problem dimension.

by an order of magnitude should be expected as discussed in [34]); ii) as discussed in [21], the polynomial approach relies on a low order quadratic approximation at each point of the predicted trajectory in order to represent the polynomial constraint in CVXPY more efficiently; iii) performance depends on the hyperparameters for a given decomposition (e.g. a larger number of RBF functions means more computational burden).

We conclude from this subsection that using polynomial decomposition results in optimization problems with shorter computation time and yields faster convergence of the closed loop to the reference and smaller steady state errors.

6.4 Effect of additive disturbance

The PVTOL aircraft was subject to a random additive disturbance following a uniform distribution $\mathcal{U}(-0.1, 0.1)$ and acting on the horizontal and vertical velocity dynamics. The time response of the closed loop is illustrated in Figure 11 with corresponding disturbance magnitude, showing the satisfying disturbance rejection capabilities of the controller (neural-network-based decomposition, $N = 50$, $\delta = 0.5$ s). Figure 12 shows similarly good disturbance rejection is observed even when being robust to neural network modelling errors (see Section 4.5).

The magnitude of the disturbance can be increased further if a backtracking line search scheme is implemented as discussed in Section 4 in order to prevent infeasible initial states induced by the disturbance. To demonstrate the possibility of recovering from infeasible optimization problems, the maximum allowable magnitude of the disturbance was multiplied by 10 and the system was simulated with initial line search parameter $\rho = 0.2$. The optimization was found to be infeasible at 8 different iterations but the backtracking scheme always reinitialized

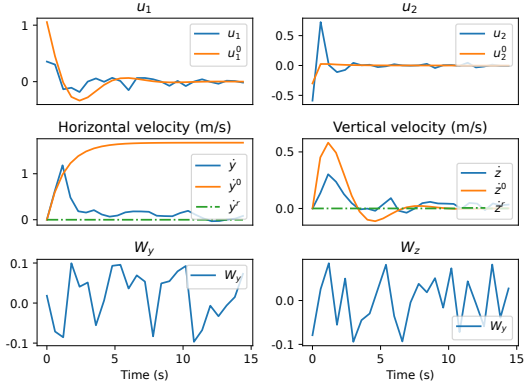


Figure 11: Closed-loop response with additive disturbance.

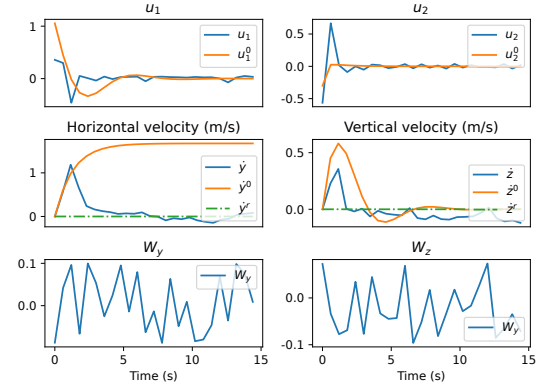


Figure 12: Closed-loop response with additive disturbance, robust to neural network modelling errors.

the problem with a feasible trajectory given by equation (22) after 1-2 iterations of the scheme, allowing the algorithm to resume. Since the sets \mathcal{X} and \mathcal{U} are defined via elementwise bounds, the performance of the backtracking algorithm is evaluated using the relaxation objective $J_{\mathcal{X},\mathcal{U}} := \min_{\bar{\mathcal{X}}, \underline{\mathcal{X}}, \bar{\mathcal{U}}, \underline{\mathcal{U}}} \|\bar{\mathcal{X}} + \underline{\mathcal{X}}\|_Q + \|\bar{\mathcal{U}} + \underline{\mathcal{U}}\|_R$, where $\bar{\mathcal{X}}, \underline{\mathcal{X}}, \bar{\mathcal{U}}, \underline{\mathcal{U}}$ are elementwise nonnegative relaxations of the sets \mathcal{X} and \mathcal{U} . At each iteration of the backtracking algorithm, these relaxations are selected such that the corresponding relaxed problem (23) is feasible. The objective $J_{\mathcal{X},\mathcal{U}}$ is a measure of the minimum relaxation required in the constraints for the problem to become feasible. When it becomes small enough, the problem is found to be feasible without any relaxation. Results for this run are presented in Table 1, which shows a total of 8 infeasibility detections, all of which were recovered from using the proposed backtracking line search approach. The time step and iteration at which an infeasibility event is recorded are denoted by n and i , respectively. The total number of backtracking iterations required to regain feasibility is denoted by \mathcal{B} , and the initial and final values

n	i	\mathcal{B}	$J_{\mathcal{X},\mathcal{U}}^0$	$J_{\mathcal{X},\mathcal{U}}^{\mathcal{B}}$
2	2	2	5.0250×10^{-4}	7.7796×10^{-8}
10	3	1	1.3031×10^{-4}	6.5674×10^{-9}
10	4	1	1.3620×10^{-4}	1.8534×10^{-8}
10	5	1	1.2475×10^{-4}	7.7934×10^{-8}
13	1	1	4.3111×10^{-4}	1.5087×10^{-7}
13	4	1	1.4110×10^{-2}	1.4308×10^{-7}
13	5	1	1.4315×10^{-2}	2.9371×10^{-8}
22	5	1	4.1392×10^{-4}	1.2096×10^{-7}

Tab. 1: $J_{\mathcal{X},\mathcal{U}}^0$ and $J_{\mathcal{X},\mathcal{U}}^{\mathcal{B}}$ for all infeasibility detections.

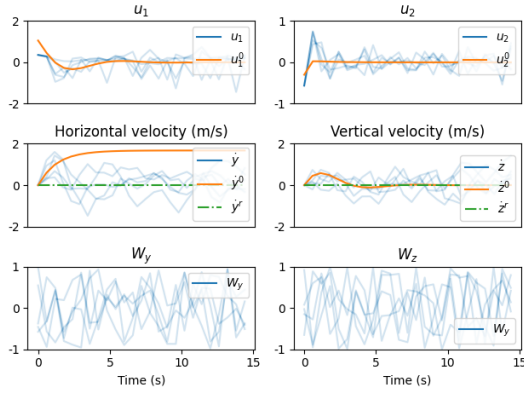


Fig. 13: Closed-loop response for five runs with a unit maximum additive disturbance magnitude and **maxIters** = 1.

of $J_{\mathcal{X},\mathcal{U}}$ are denoted by $J_{\mathcal{X},\mathcal{U}}^0$ and $J_{\mathcal{X},\mathcal{U}}^{\mathcal{B}}$, respectively.

Under resource-constrained environments, it may also be useful to run the algorithm with **maxIters** = 1, which in the modified algorithm is similar to running with $\rho \rightarrow 1$, as explained in Section 4.4. The spread for five successful runs with a unit maximum allowable disturbance magnitude is presented in Figure 13, which still shows disturbance rejection despite the order-of-magnitude increase in disturbance bounds.

6.5 Early termination property

A key property of the MPC scheme presented in this paper is that the successive linearization procedure at each time step (i.e. the "while" loop in line 12 of Algorithms 1 or 2) can be terminated early—in particular after only one iteration—without compromising stability under the MPC law. This is a direct consequence of the recursive feasibility property established in propositions 2 and 6, Section 5 for the nominal and disturbed cases respectively. In Figures 14 and 15, we compare the impact of early termination on the closed loop response and the objective evolution over time for the PVTOL aircraft with

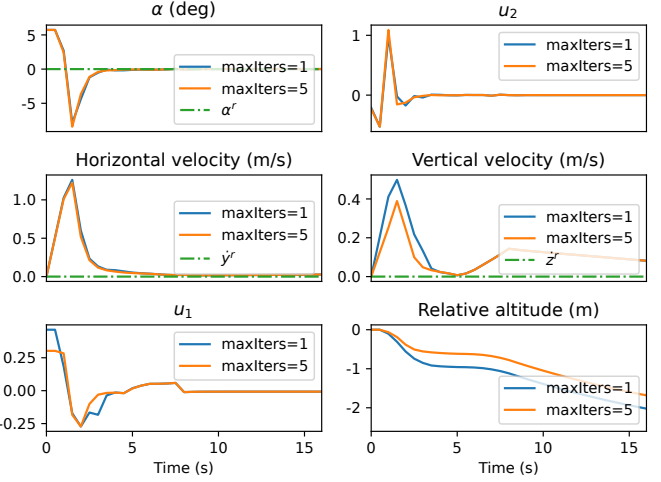


Fig. 14: Comparison of closed-loop solution for different maximum iterations per time step.

neural-network-based decomposition, simplex tube cross sections, $N = 50$, $\delta = 0.5$ s. The blue curves correspond to results obtained with **maxIters** = 1 and the orange curves correspond to **maxIters** = 5. It is plain that although more iterations per time step yield better convergence, the gain is not noticeable enough to compensate for the computational overhead of multiple iterations. In fact, the results obtained with a single iteration per time step are satisfying in this scenario and potentially more complex ones as shown in [18].

7 Conclusion

This paper has introduced a computationally tractable robust MPC algorithm for nonlinear systems with continuous dynamics. The method relies on a difference-of-convex (DC) decomposition of the dynamics, successive linearizations and robust stabilization of the closed loop via a tube-based MPC scheme that treats linearization errors as bounded disturbances. Exploiting convexity in the DC dynamics, these disturbances are necessarily convex and tight, which allows deriving the control law as the solution of a sequence of convex programs with predictable computational effort.

We have shown that the DC decomposition can be obtained by various means, using algebraic techniques such as sum-of-squares polynomials or machine learning methods such as convex radial basis functions approximations and input-convex neural networks. We have presented a computationally efficient tube-based MPC algorithm to solve the robust control problem once the dynamics are expressed in DC form. Two tube parameterizations are

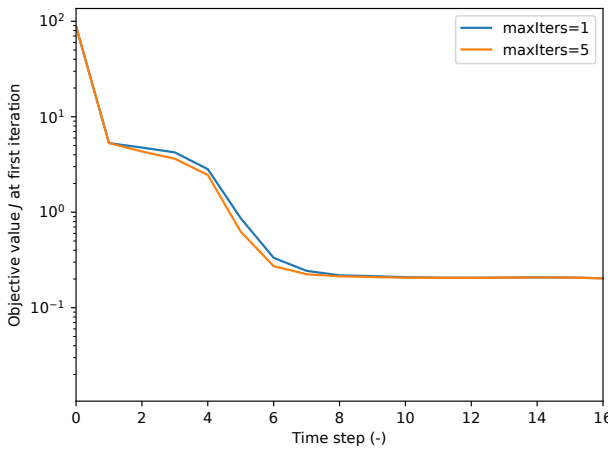


Fig. 15: Comparison of objective evolution for different maximum iterations per time step.

proposed, relying on simplex and elementwise bounds. We have demonstrated theoretical results such as recursive feasibility, convergence, and asymptotic stability. These results were generalized in the presence of external disturbances. Finally, we have conducted numerical simulations and analysed the performances of the algorithm in a PVTOL aircraft case study.

Results show that the polynomial DC decomposition is superior to others in terms of accuracy, convergence and computation time. The simplex parameterization of the tube is the most computationally efficient. Crucially, the scheme we propose can be terminated early after only one iteration per time step without affecting stability, which makes our method attractive in real-time applications. The preliminary results with the CVXPY generic convex optimization package are promising and suggest excellent scalability if specific solvers are developed. In particular, when the dynamics are decomposed in DC form using input-convex neural networks with ReLU activation, the nonlinear tube MPC optimization problem could be reformulated as a linear program. This would represent a notable progress in terms of computation time and would pave the way for real-time state-of-the-art implementations of nonlinear robust MPC. Another future direction will consider the use of convex recurrent neural network architectures to learn the system trajectories in DC form over the prediction horizon, which represents an alternative to learning the dynamic function and will expand the toolbox of available DC decompositions. Finally, we note that the proposed DC-based successive convexification framework is not specific to receding-horizon control and can be applied to single-shot nonlinear optimization problems with continuous constraints. We will investigate applications of the proposed method to problems in

urban air mobility, sustainable aviation, and energy systems, where robust handling of nonlinear dynamics and uncertainty under real-time computational constraints is essential.

A Feedback gain computation

The gains $\{K_k\}_{k=0}^{N-1}$ in equation (3) can be computed e.g. using a dynamic programming (DP) recursion initialized with $P_N = \hat{Q}$, and defined for $k = N-1, \dots, 0$ by

$$\begin{aligned}\Delta_k &= B_k^\top P_{k+1} B_k + R, \\ K_k &= -\Delta_k^{-1} B_k^\top P_{k+1} A_k, \\ P_k &= Q + A_k^\top P_{k+1} A_k - A_k^\top P_{k+1} B_k \Delta_k^{-1} B_k^\top P_{k+1} A_k,\end{aligned}\quad (25)$$

where $A_k = \frac{\partial f}{\partial x}(x_k^\circ, u_k^\circ)$, $B_k = \frac{\partial f}{\partial u}(x_k^\circ, u_k^\circ)$.

B Terminal parameters

We summarize here a method for computing the terminal gain \hat{K} , terminal weighting matrix \hat{Q} , terminal set $\hat{\mathcal{X}}$ and terminal set bound $\hat{\gamma}$ for the TMPC problem of Section 3 by solving a semidefinite program (SDP).

To ensure convergence⁴, the terminal weighting matrix $\hat{Q} \succ 0$ is chosen so that, for all $x \in \hat{\mathcal{X}}$,

$$\begin{aligned}\|x - x^r\|_{\hat{Q}}^2 &\geq \|f(x, \hat{K}(x - x^r) + u^r) - x^r\|_{\hat{Q}}^2 \\ &\quad + \|x - x^r\|_Q^2 + \|\hat{K}(x - x^r)\|_R^2,\end{aligned}\quad (26)$$

where the terminal set $\hat{\mathcal{X}}$ and feedback gain \hat{K} satisfy

$$\hat{\mathcal{X}} \subseteq \mathcal{X}, \quad \hat{K}\hat{\mathcal{X}} \oplus \{u^r - \hat{K}x^r\} \subseteq \mathcal{U}. \quad (27)$$

The terminal set can be defined, for example, as

$$\hat{\mathcal{X}} = \{x : \|x\|_{\hat{Q}}^2 \leq \hat{\gamma}\} \quad (28)$$

Given bounds $\bar{\mathcal{X}} = \{x : |x - x^r| \leq \delta^x\} \subseteq \mathcal{X}$, $\bar{\mathcal{U}} = \{u : |u - u^r| \leq \delta^u\} \subseteq \mathcal{U}$ on the state and control input within the terminal set, we assume that the nonlinear system dynamics (1) can be represented in $\bar{\mathcal{X}} \times \bar{\mathcal{U}}$ using a set of linear models. The model approximation is assumed to satisfy, for all k ,

$$\begin{aligned}f(x, u) - f(x^r, u^r) &\in \text{Co}\{A^{(i)}(x - x_k^r) + B^{(i)}(u - u_k^r), \\ i &= 1, \dots, m\}, \quad \forall (x, u) \in \bar{\mathcal{X}} \times \bar{\mathcal{U}}\end{aligned}\quad (29)$$

where Co denotes the convex hull. In order that \hat{Q} and \hat{K} satisfy the inequality (26) we require, for all $x \in \bar{\mathcal{X}}$,

⁴Equation (26) can be seen as a descent property for the Lyapunov function $V(x - x^r) = \|x - x^r\|_{\hat{Q}}^2$.

$$\begin{aligned}\|x - x^r\|_{\hat{Q}}^2 &\geq \|A^{(i)}(x - x^r) + B^{(i)}\hat{K}(x - x^r)\|_{\hat{Q}}^2 \\ &\quad + \|x - x^r\|_Q^2 + \|\hat{K}(x - x^r)\|_R^2.\end{aligned}$$

Since each term is quadratic in $x - x^r$, this condition is equivalent to a set of matrix inequalities, for $i = 1, \dots, m$,

$$\hat{Q} \succeq (A^{(i)} + B^{(i)}\hat{K})^\top \hat{Q}(A^{(i)} + B^{(i)}\hat{K}) + Q + \hat{K}^\top R \hat{K},$$

which can be expressed equivalently using Schur complements as LMIs in variables $S = \hat{Q}^{-1}$ and $Y = \hat{K}\hat{Q}^{-1}$:

$$\begin{bmatrix} S & (A^{(i)}S + B^{(i)}Y)^\top & S & Y^\top \\ \star & S & 0 & 0 \\ \star & \star & Q^{-1} & 0 \\ \star & \star & \star & R^{-1} \end{bmatrix} \succeq 0, \quad i = 1, \dots, m. \quad (30)$$

To ensure that the model approximation (29) remains valid we can exploit the positive invariance of the set $\hat{\mathcal{X}} = \{x : \|x - x^r\|_{\hat{Q}} \leq \hat{\gamma}\}$ for all $\hat{\gamma} > 0$, and impose the constraints

$$\{x : \|x - x^r\|_{\hat{Q}}^2 \leq \hat{\gamma}\} \subseteq \bar{\mathcal{X}} \cap \{x : Kx \in \bar{\mathcal{U}}\}$$

which are equivalent to

$$\hat{\gamma}^{-1}[\delta^x]_i^2 - [S]_{ii} \succeq 0, \quad i = 1, \dots, n_x \quad (31)$$

$$\begin{bmatrix} \hat{\gamma}^{-1}[\delta^u]_i^2 & [Y]_i \\ \star & S \end{bmatrix} \succeq 0, \quad i = 1, \dots, n_u \quad (32)$$

To balance the requirements for good terminal controller performance and a large terminal set, we can minimize $\text{tr}(\hat{Q}) + \alpha\hat{\gamma}^{-1}$ subject to constraints (30), (31), (32) and

$$\begin{bmatrix} S & I \\ \star & \hat{Q} \end{bmatrix} \succ 0, \quad (33)$$

over variables $S = S^\top$, Y and $\hat{\gamma}^{-1}$, where α is a scalar constant that controls the trade-off between the competing objectives of minimizing $\text{tr}(\hat{Q})$ and minimizing $\hat{\gamma}^{-1}$.

C Maximum of a convex function defined on a polytope

Theorem 8 (Maximum of a convex function). *The maximum of a convex function f defined over a polytopic set $\mathcal{P} = \text{Co}\{v_1, \dots, v_m\}$ is achieved at one of its vertices v_1, \dots, v_m , i.e.*

$$\max_{x \in \mathcal{P}} f(x) = \max\{f(v_1), \dots, f(v_m)\}.$$

Proof. Since $\mathcal{P} = \text{Co}\{v_1, \dots, v_m\}$, any $x \in \mathcal{P}$ can be expressed as a convex combination of the vertices as follows $x = \sum_{i=1}^m \lambda_i v_i$ for some positive λ_i that form a partition of unity. By convexity of f , we have

$$f(x) \leq \sum_{i=1}^m \lambda_i f(v_i) \leq \max_i \{f(v_i)\},$$

which is valid $\forall x \in \mathcal{P}$ and achieves the proof. \square

D Linearization

In Section 3, the DC constraints in equation (6) are linearized to obtain the convex constraints $g(x_k, u_k) - \lfloor h^\circ \rfloor(x_k, u_k) \leq q_{k+1}$ in equation (7) where $\lfloor h^\circ \rfloor(x_k, u_k) = h(x_k^\circ, u_k^\circ) + A_k(x_k - x_k^\circ) + B_k(u_k - u_k^\circ)$ and A_k, B_k are the matrices of the state space linearization of h at (x_k°, u_k°) . We now discuss the form taken by these matrices depending on the specific DC decomposition. In what follows we denote $x = [x_k^\top \quad u_k^\top]^\top$ and $x^\circ = [x_k^{\circ\top} \quad u_k^{\circ\top}]^\top$.

D.1 SOS-convex Polynomials

Assuming $h = [y^\top H_1 y, \dots, y^\top H_{n_x} y]^\top$, the state-space linearized system is given by

$$[A_k]_{lj} = y(x_k^\circ, u_k^\circ)^\top (D_{x,j}^\top H_l + H_l D_{x,j}) y(x_k^\circ, u_k^\circ),$$

$$[B_k]_{lj} = y(x_k^\circ, u_k^\circ)^\top (D_{u,j}^\top H_l + H_l D_{u,j}) y(x_k^\circ, u_k^\circ),$$

where we denote $\partial y / \partial [x_k]_j = D_{x,j} y$, $\partial y / \partial [u_k]_j = D_{u,j} y$.

D.2 Input-convex neural networks

Let h be approximated by an L -layer ICNN: $h = (\sigma \circ \mathcal{A}_{\theta_{L-1},x} \circ \dots \circ \sigma \circ \mathcal{A}_{\theta_1,x} \circ \sigma \circ \mathcal{A}_{\Phi_0})(x)$. The chain rule can be used to compute the first order derivative of the network as follows

$$\begin{aligned}\frac{\partial h}{\partial x}(x; \theta) &= (\sigma' \circ \mathcal{A}_{\theta_{L-1},x} \circ \dots \circ \sigma \circ \mathcal{A}_{\Phi_0})(x) \cdot (\mathcal{A}'_{\theta_{L-1},x} \circ \dots \\ &\quad \circ (\sigma' \circ \mathcal{A}_{\theta_1,x} \circ \sigma \circ \mathcal{A}_{\Phi_0})(x) \cdot (\mathcal{A}'_{\theta_1,x} \circ \sigma \circ \mathcal{A}_{\Phi_0})(x) \\ &\quad \circ (\sigma' \circ \mathcal{A}_{\Phi_0})(x) \cdot \mathcal{A}'_{\Phi_0}(x)), \quad (34)\end{aligned}$$

where $\mathcal{A}'_{\theta_l,x}(z) = \Theta_l z + \Phi_l$, $\forall l \in \{1, \dots, L-1\}$, $\mathcal{A}'_{\Phi_0} = \Phi_0$, and in the case of ReLU activation, $\sigma'(x) = \text{diag}\{H(x_1), H(x_2), \dots\}$ where $H(\cdot)$ is the Heaviside step function.

Example 2. Consider an ICNN with $L = 2$ and partitioning $\Phi_l = [\Phi_{l,x_k} \mid \Phi_{l,u_k}]$, $\forall l \in \{0, 1\}$, where $\Phi_{l,x_k} \in \mathbb{R}^{n_l \times n_x}$, $\Phi_{l,u_k} \in \mathbb{R}^{n_l \times n_u}$, the A_k, B_k matrices of the state space linearization are given by

$$A_k = \frac{\partial h}{\partial x_k}(x_k^\circ, u_k^\circ; \theta) = \sigma'(a_1)(\Theta_1 \sigma'(a_0)\Phi_{0,x_k} + \Phi_{1,x_k}),$$

$$B_k = \frac{\partial h}{\partial u_k}(x_k^\circ, u_k^\circ; \theta) = \sigma'(a_1)(\Theta_1 \sigma'(a_0)\Phi_{0,u_k} + \Phi_{1,u_k}),$$

where $a_1 = \Theta_1 \sigma(\Phi_{0,x_k} x_k^\circ + \Phi_{0,u_k} u_k^\circ + b_0) + \Phi_{1,x_k} x_k^\circ + \Phi_{1,u_k} u_k^\circ + b_1$ and $a_0 = \Phi_{0,x_k} x_k^\circ + \Phi_{0,u_k} u_k^\circ + b_0$.

D.3 Radial basis functions

Let h be approximated as a weighted sum of convex RBF: $h = \sum_{j=1}^m \alpha_j \sqrt{1 + \rho_j^2(x - c_j)^\top (x - c_j)}$. Partition-

ing $c_j = [c_{x,j}^\top \ c_{u,j}^\top]^\top$, the A_k, B_k matrices of the state space linearization of h at (x_k°, u_k°) are given by

$$A_k = \sum_{j=1} \frac{\rho_j^2 \alpha_j (x_k^\circ - c_{x,j})^\top}{\sqrt{1 + \rho_j^2 (x^\circ - c_j)^\top (x^\circ - c_j)}},$$

$$B_k = \sum_{j=1} \frac{\rho_j^2 \alpha_j (u_k^\circ - c_{u,j})^\top}{\sqrt{1 + \rho_j^2 (x^\circ - c_j)^\top (x^\circ - c_j)}}.$$

References

[1] James Blake Rawlings, David Q Mayne, and Moritz Diehl. *Model predictive control: theory, computation, and design*. Nob Hill Publishing Madison, WI, 2 edition, 2017.

[2] Basil Kouvaritakis and Mark Cannon. Model predictive control. *Switzerland: Springer International Publishing*, 2016.

[3] David Q Mayne, María M Seron, and SV Raković. Robust model predictive control of constrained linear systems with bounded disturbances. *Automatica*, 41(2):219–224, 2005.

[4] David Q Mayne, Erric C Kerrigan, E. J. van Wyk, and Paola Falugi. Tube-based robust nonlinear model predictive control. *International Journal of Robust and Nonlinear Control*, 21(11):1341–1353, 2011.

[5] Brett T Lopez, Jonathan P How, and Jean-Jacques E Slotine. Dynamic tube MPC for nonlinear systems. In *2019 American Control Conference (ACC)*, pages 1655–1662. IEEE, 2019.

[6] Johannes Köhler, Peter Kötting, Raffaele Soloperto, Frank Allgöwer, and Matthias Müller. A robust adaptive model predictive control framework for nonlinear uncertain systems. *International Journal of Robust and Nonlinear Control*, 31:8725–8749, 2021.

[7] András Sasfi, Melanie N. Zeilinger, and Johannes Köhler. Robust adaptive MPC using control contraction metrics. *Automatica*, 155:111169, 2023.

[8] L.T. Biegler. Advances in nonlinear programming concepts for process control. *Journal of Process Control*, 8(5):301–311, 1998.

[9] Young Il Lee, Basil Kouvaritakis, and Mark Cannon. Constrained receding horizon predictive control for nonlinear systems. *Automatica*, 38(12):2093–2102, 2002.

[10] A.P. Leeman, J. Sieber, S. Bennani, and M.N. Zeilinger. Robust optimal control for nonlinear systems with parametric uncertainties via system level synthesis. In *62nd IEEE Conference on Decision and Control (CDC)*, pages 4784–4791, Singapore, 2023.

[11] Mark Cannon, Johannes Buerger, Basil Kouvari- takis, and Saša Raković. Robust tubes in nonlinear model predictive control. *IEEE Transactions on Automatic Control*, 56(8):1942–1947, 2011.

[12] J. Buerger and M. Cannon. Safe adaptive NMPC using ellipsoidal tubes. In *European Control Conference, Thessaloniki, Greece*, 2025.

[13] Florian Messerer, Katrin Baumgärtner, and Moritz Diehl. Survey of sequential convex programming and generalized Gauss-Newton methods. *ESAIM: ProcS*, 71:64–88, 2021.

[14] Martin Doff-Sotta and Mark Cannon. Difference of convex functions in robust tube nonlinear MPC. In *IEEE 61st conference on decision and control (CDC)*, pages 3044–3050, 2022.

[15] G.R.G. Lanckreit and Sriperumbudur B.K. On the convergence of the concave-convex procedure. In *Advances in Neural Information Processing Systems 22 (NIPS 2009)*, pages 1759–1767, 2009.

[16] Thomas Lipp and Stephen Boyd. Variations and extension of the convex-concave procedure. *Optimization and Engineering*, 17(2):263–287, 2016.

[17] Yana Lishkova and Mark Cannon. Robust receding horizon control for convex dynamics and bounded disturbances. *IEEE Transactions on Automatic Control*, 70(10):6436–6448, 2025.

[18] Martin Doff-Sotta. *Optimisation and control of aerospace vehicles*. PhD thesis, University of Oxford, 2023.

[19] Johannes Buerger, Mark Cannon, and Martin Doff-Sotta. Safe learning in nonlinear model predictive control. In *6th Annual Conference on Learning for Dynamics and Control (L4DC)*. University of Oxford, 2024.

[20] Philip Hartman. On functions representable as a difference of convex functions. *Pacific Journal of Mathematics*, 9(3):707–713, 1959.

[21] Martin Doff-Sotta, Mark Cannon, and Marko Bacic. Robust trajectory optimisation for transitions of tiltwing VTOL aircraft. In *IEEE Conference on Control Technology and Applications (CCTA)*, pages 425–431. IEEE, 2023.

[22] M. Doff-Sotta, M. Cannon, and M. Bacic. Data-driven robust model predictive control of tiltwing vertical take-off and landing aircraft. *Journal of Guidance Control and Dynamics*, 48(1):203–211, 2024.

[23] Niels Krausch, Martin Doff-Sotta, Mark Cannon, Peter Neubauer, and Mariano Nicolas Cruz-Bournazou. Handling nonlinearities and uncertainties of fedbatch cultivations with difference of convex functions tube MPC. In *Computer Aided Chemical Engineering*, volume 53, pages 1699–1704. Elsevier, 2024.

[24] N. Krausch, M. Doff-Sotta, M. Cannon, P. Neubauer, and M.N. Cruz Bournazou. Deep

learning adaptive model predictive control of fed-batch cultivations. *Computers and Chemical Engineering*, 203:109344, 2025.

[25] S. Steffen and M. Cannon. Deep Learning Model Predictive Control for Deep Brain Stimulation in Parkinson’s Disease. In *64th IEEE Conference on Decision and Control*, 2025.

[26] R. Horst and N.V. Thoai. DC programming: Overview. *Journal of Optimization Theory and Applications*, 103(1):1–43, 1999.

[27] Amir Ali Ahmadi and Georgina Hall. DC decomposition of nonconvex polynomials with algebraic techniques. *Mathematical Programming*, 169(1):69–94, 2018.

[28] Brandon Amos, Lei Xu, and J Zico Kolter. Input convex neural networks. In *International Conference on Machine Learning*, pages 146–155. PMLR, 2017.

[29] Stephen P Boyd and Lieven Vandenberghe. *Convex optimization*. Cambridge university press, 2004.

[30] Parameswaran Sankaranarayanan and Raghunathan Rengaswamy. CDiNN-convex difference neural networks. *Neurocomputing*, 495:153–168, 2022.

[31] Trevor Hastie, Robert Tibshirani, Jerome H Friedman, and Jerome H Friedman. *The elements of statistical learning: data mining, inference, and prediction*, volume 2. Springer, 2009.

[32] Vincent Delos and Denis Teissandier. Minkowski Sum of Polytopes Defined by Their Vertices. *Journal of Applied Mathematics and Physics*, 3(1):62–67, January 2015. doi: 10.4236/jamp.2015.31008.

[33] François Chollet et al. Keras. <https://keras.io>, 2015.

[34] Martin Doff-Sotta, Mark Cannon, and Marko Bacic. Predictive energy management for hybrid electric aircraft propulsion systems. *IEEE Transactions on Control Systems Technology*, 31(2):602–614, 2022.